Measurement of Cross Sections for X-Ray Production by High-Energy Electrons*

L. M. Middleman, R. L. Ford, and R. Hofstadter
Department of Physics and High Energy Physics Laboratory, Stanford University, Stanford, California 94305
(Received 13 March 1970)

Using high-resolution semiconductor detectors, a study was made of the large K-ionization cross sections of atoms over a wide range of atomic numbers ($Z=29-83$) and of incident electron energies ($E=150-900$ MeV). For the higher-Z elements ($Z>60$), the L x-ray cross sections were also measured over the incident electron energy range. Ratios of the relative intensities of various distinct lines were determined and compared to recent low-energy work. The results of the K-ionization experiment are compared to the recent relativistic calculations of Kolbenstvedt. The experimental K-ionization cross sections for each incident electron energy appear to fit a power-law dependence on the atomic number. The Kolbenstvedt theory also exhibits a power-law dependence and is in good agreement with this experiment. All differential x-ray cross sections were found to be isotropic. The L x-ray cross sections measured for four high-Z elements increase with atomic number and incident electron energy. The $L\beta/L\alpha$, $L\gamma/L\alpha$, and K/L intensity ratios are also given. A search for nuclear γ rays produced by high-energy electron scattering was also undertaken in this work. No nuclear γ-ray lines were detected. Recent theoretical calculations show that the expected cross sections are below the minimum observable levels in these experiments. However, a 511-keV γ line was observed. This line was associated with positron annihilation and was apparently produced in the target.

I. INTRODUCTION

The availability of high-resolution semiconductor photon detectors furnished an interesting and unique opportunity to study x-ray and γ-ray spectra from solid targets excited by high-energy electron bombardment. Figure 1 shows some of the possibilities permitted by this new technique.

This investigation consisted of two phases. The first involved the construction and adaptation of a semiconductor x-ray and γ-ray detector system for the Mark-III accelerator at Stanford. This work was followed by a second phase which involved the development of shielding and timing techniques and the subsequent x-ray and γ-ray experiments. The experiments performed in this work were confined to the observation of photons with energies between 5 keV and 2 MeV.

A. X-Ray Studies

The K-ionization cross sections from electron bombardment have previously been investigated for incident electron energies up to 2 MeV. Reviews of the results of these investigations were given in work by Motz and Placious, [1] and by Kolbenstvedt. [2] These experiments were performed for only a few atomic numbers, and there exist discrepancies between the various works and between experimental results and existing theories.

This experiment was performed over a wide range of atomic numbers and for incident energies of 150, 300, 500, 700, and 900 MeV. By extending the incident electron energy into this ultrarelativistic range, the experiment yielded further information on the energy-loss and energy-transfer mechanisms at high energy. A comparison of the results with theoretical calculations provides a test of the approximation techniques required in calculations of high-energy interactions.

The targets used were $_{29}$Cu, $_{38}$Sr, $_{42}$Mo, $_{49}$In, $_{69}$Tm, $_{73}$Ta, $_{79}$Au, and $_{83}$Bi. With the good energy resolution of the semiconductor detectors [for the Si(Li) detectors, full width at half-maximum = 430 eV at 14.4 keV], the $K\alpha/K\beta$ intensity ratio was also measured for these targets over this energy range. For the highest-Z elements used ($_{73}$Ta, $_{79}$Au, and $_{83}$Bi), the $K\alpha_1/K\alpha_2$ and $K\beta_1'/K\beta_2'$ intensity ratios were also measured.

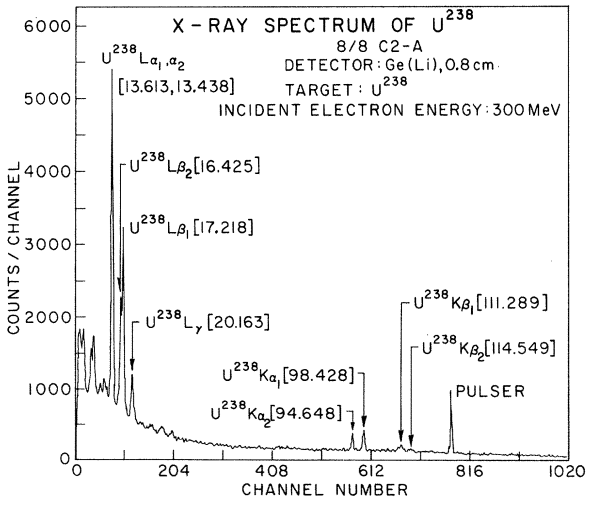

FIG. 1. X-ray spectrum of U^{238} taken during initial studies.

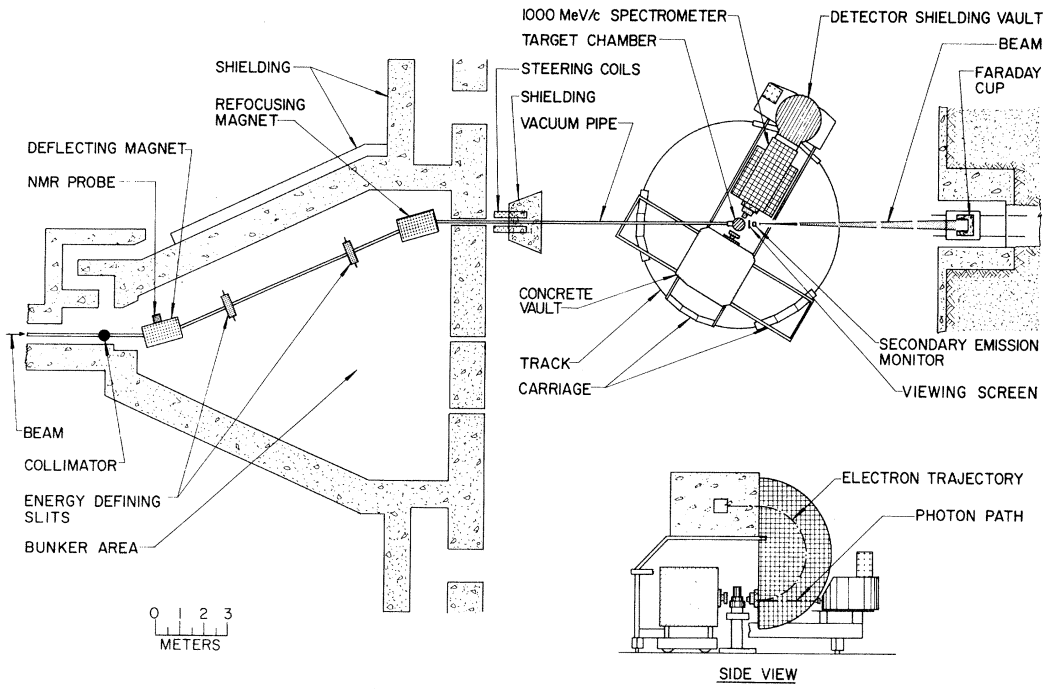

FIG. 2. Plan view of the beam-analyzing system and the target area.

In addition, the L x-ray cross sections were measured for the four high-Z elements, and the $L\beta/L\alpha$, $L\gamma/L\alpha$, and K/L intensity ratios were determined.

B. γ-Ray Studies

A search for nuclear γ rays produced by high-energy electron scattering was also undertaken in this work. Several target elements were chosen whose nuclei have energies of excited states of less than 2 MeV.

Griffy[3] has made preliminary calculations for the expected total cross section for excitation of the $E2$ transition in Ta^{181}. The initial search for nuclear lines in Ta and Au was made and no lines were detected with the exception of the 0.511-MeV positron annihilation line. By observing this γ line, estimates could be made of the minimum cross sections which would be detectable for the conditions of solid angle, background, noise, duty cycle of the accelerator, and time limitation. This work combined with more recent calculations by Whitehill and Griffy[4] provides estimates for possible future measurements.

II. EQUIPMENT

To coordinate this experiment with others already in progress on the Mark-III accelerator, the existing facilities were used. For this reason the shielding vault of the detector system was mounted behind the 72-in. 180° double-focusing spectrometer magnet. This layout, shown in Fig. 2, provided additional shielding of the detector electronic equipment from background radiation and scattered particles, as well as a sweeping magnet to remove background charged particles.

The general configuration of the experiment is shown in Fig. 3. The concrete vault mounted opposite the 72-in. magnet was also used for the γ-ray experiment. The two photon detectors used in these experiments were cooled lithium-drifted semiconductor detectors. A 1-cm^3 lithium-drifted germanium Ge(Li) detector was used for the γ-ray search and for the higher-Z x-ray studies. The 0.3-cm-deep Si(Li) detector was used for all low-energy x-ray studies. Figure 4 is a complete schematic diagram of a detector cryostat.

The preamplifiers in these detector systems used the high-resolution high-rate design of Goulding. The complete detection and analysis system is shown in Fig. 5. A description of the data storage system is given elsewhere.[5]

A complete calibration of the linearity of the detector system was performed prior to these experiments. The linearity studies performed on each detector and on the entire electronic system were reported earlier.[6] In addition, energy-resolution and detection-efficiency studies were carried out.[5] Figures 6 and 7 depict the absolute photopeak efficiencies of the Si(Li) and Ge(Li) detectors,

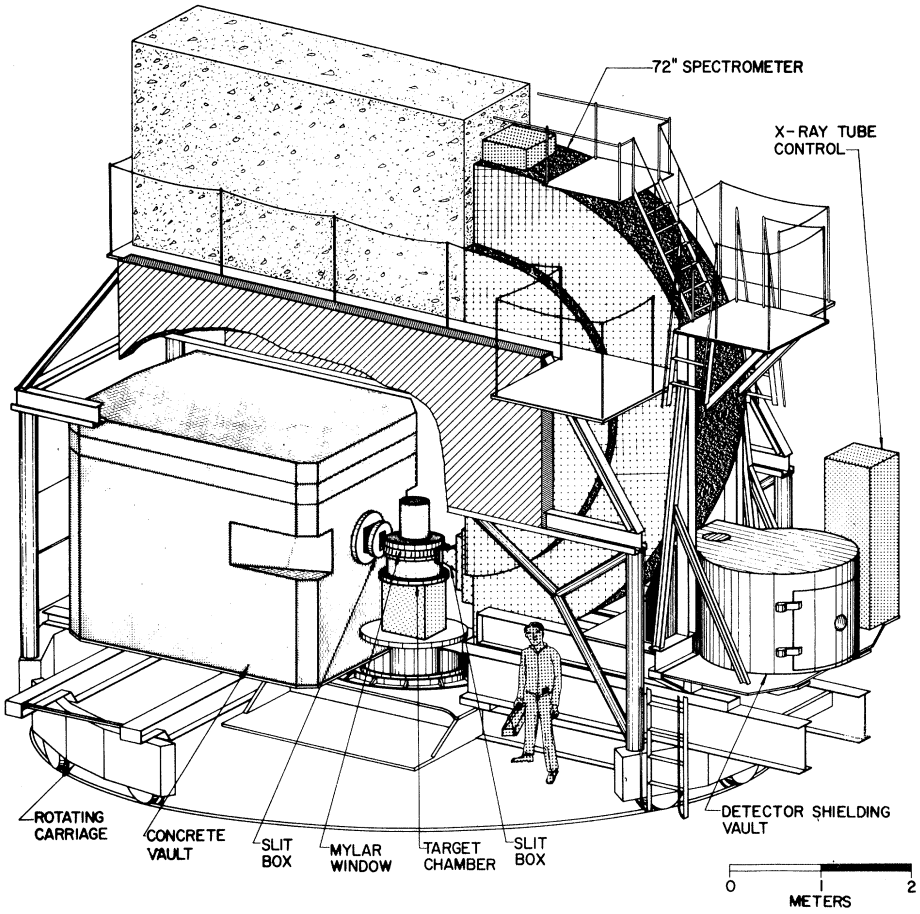

FIG. 3. Perspective view of the spectrometer system.

respectively. The absolute calibration method has been described earlier.[5] The Ge(Li) detector efficiency curve has not been corrected for the escape of Ge K x rays; thus, the photopeak efficiency decreases rapidly below 35 keV (Fig. 7). This detector was not normally used for x-ray studies below 50 keV.

Where possible, single isotopes were chosen as targets. The targets were usually 99.99% pure and were typically between 1000 and 5000 Å thick. By using thin targets, K ionization produced by target bremsstrahlung and secondary electrons was minimized. Self-absorption of x rays was less than 2% in these thin targets, and a high-intensity stable electron beam could be used. Targets of $_{29}$Cu, $_{38}$Sr, $_{49}$In, $_{69}$Tm, $_{79}$Au, and $_{83}$Bi were produced by vacuum deposition. The $_{42}$Mo and $_{73}$Ta targets were produced by ion sputtering. In either procedure, the targets were deposited onto $\frac{1}{4}$-mil aluminum foil.

The anticipated low cross sections for nuclear γ rays required thicker targets. The targets used in this experiment were $_{49}In^{115}$, $_{73}Ta^{181}$, $_{79}Au^{197}$, and $_{82}$Pb, and their thicknesses ranged from 40 to 450 mg/cm^2. With Mo, Sn, Ho, or Pb absorbers placed between the detector and the target, the high intensity of target x rays was substantially reduced and the accelerator was operated at higher beam currents ($10^7 - 10^8$ electrons per pulse).

III. PROCEDURE

The detector systems, slits, and targets were aligned before each experiment using motor-driven jacks and trolleys. After each experimental run the detector cryostat was removed because of the high neutron flux associated with other high-current experiments using the accelerator. Considerable effort was spent in shielding and filtering these detector systems from the rf noise produced by the accelerator.

A. Reduction of Line-Spectra Data

The analysis program ANA used the IBM Data Acquisition and Control System 7700. For a line spectrum, a background continuum was approximated in the region of a peak by a polynomial fit to background channels outside the region of the peak. For the determination of cross sections, the

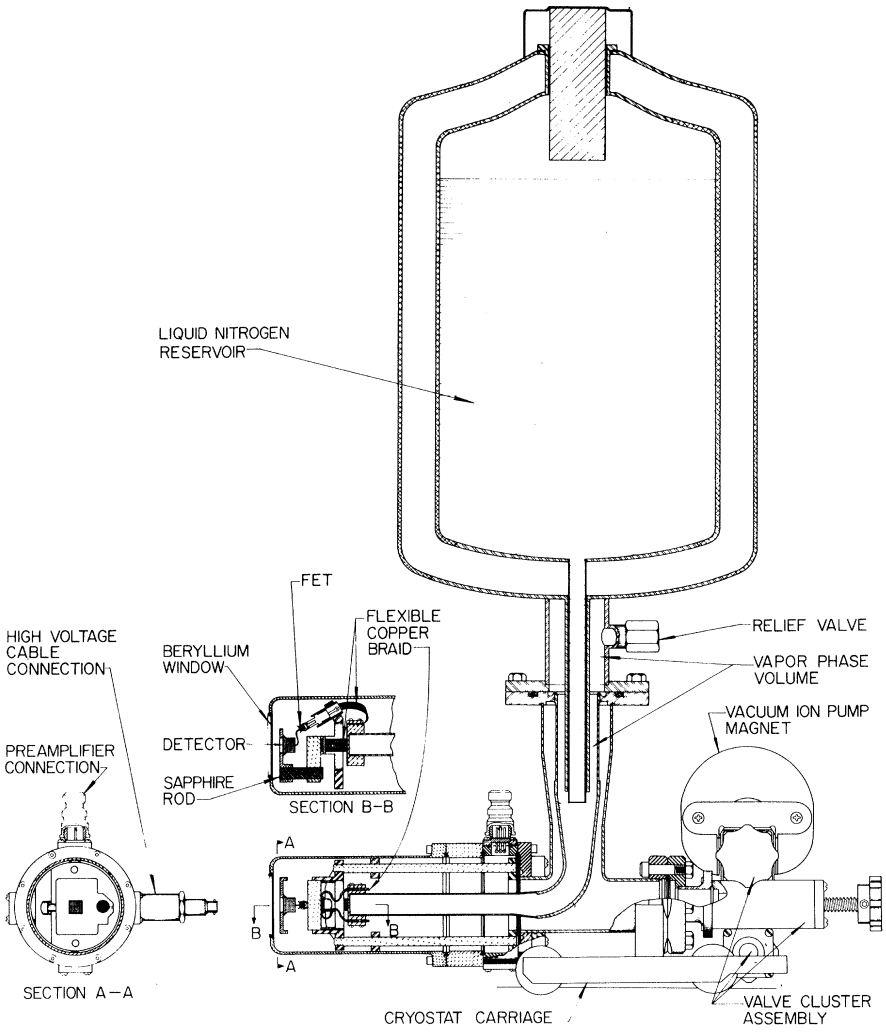

FIG. 4. Schematic diagram of the semiconductor cryostat system.

area of a full-energy peak was adequately determined by integrating the total counts in the peak after background subtraction. A thorough study of many data records showed that uncertainties in the choice of peak limits and background fit for this integration introduced little additional uncertainty to the results.[5]

The x-ray cross sections were corrected for target absorption, bremsstrahlung-induced x-ray production, and additional absorption and scattering due to materials between the target and the detector. In order to calculate the target absorption or self-absorption, it was assumed that the incident beam of electrons produced K and L ionizations uniformly along its path through the target. It was possible to make this assumption since these

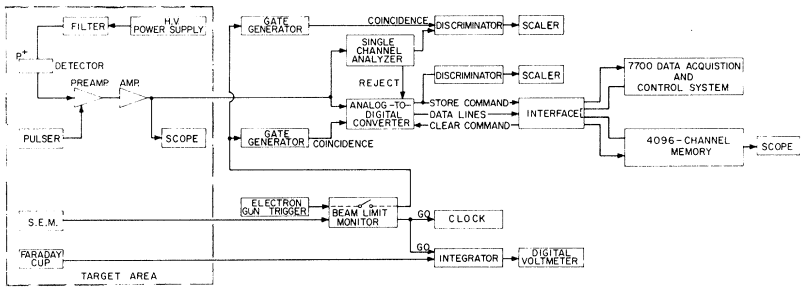

FIG. 5. Block diagram of the complete detection and analysis system. The SCA and ADC were a single commercial unit. The interface permitted the transferral of data between the 7700 system and the 4096-channel memory as well as directing the ADC output to either system.

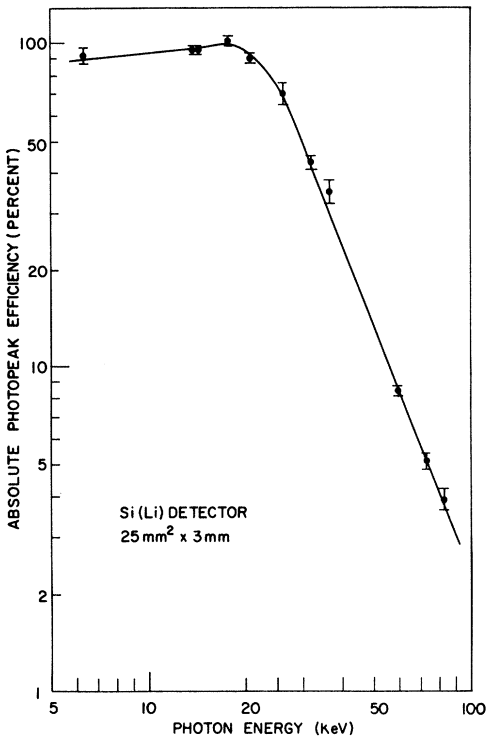

FIG. 6. Absolute photoelectric peak efficiency curve of the Si(Li) detector.

targets were less than 2 mg/cm^2 thick. A multiple Coulomb scattering calculation similar to that of Segrè[7] showed that a 100-MeV electron beam incident upon a 5-mg/cm^2 target of $_{79}$Au has a rms multiple scattering angle $\theta_{\text{rms}} = 6.5\times10^{-3}$ rad.[5] Thus, for these thin targets, the electron beam interaction throughout the target is virtually unchanged.

For photons produced uniformly in a target of thickness s, the intensity transmitted through the target is given by

$$I_{\text{trans}} = \int_0^t I_x e^{-\mu(E)d(x)}\, dx,$$

where $\mu(E)$ is the photoelectric absorption coefficient, $d(x)$ is the path length in the target for a photon produced at depth x, I_x is the uniform photon production intensity per unit length, $t = s/\cos\theta$ is the path length of the electron beam, s is the target thickness, and θ is the angle of incidence of the electron beam as measured from the normal to the target surface. Thus, the fractional target transmission is

$$T(s, Z, \varphi) = \frac{I_{\text{trans}}}{I_T} = \frac{\cos\varphi}{\mu s}\left(1 - e^{-\mu s/\cos\varphi}\right),$$

where I_T is the total intensity of photons produced in the target and φ is the viewing angle of the distant detector as measured from the surface normal. For the K-ionization experiment using the thin targets, the fractional target transmission was greater than 99%.

By using targets of various thicknesses, an attempt was made to determine the effect upon the cross sections of bremsstrahlung produced within a thin target. A comparison of the cross sections, corrected for self-absorption, of $_{29}$Cu and $_{49}$In at 300 MeV for various target thicknesses showed that the differences in the cross sections produced by different targets lie within the estimated 5% error in each thickness. Therefore, the ionization caused by bremsstrahlung produced in the target is probably small for these thin targets.

The attenuation of the x rays in air and beryllium along the path was calculated using the total absorption coefficients of Storm and Israel.[8] The attenuation in the three Mylar windows was determined by measuring the transmission intensity of various radioactive source lines.

As a result of the short duration (1.4 μsec at 60 or 120 cps) of the electron pulses on the Mark-III accelerator, the cross sections had to be corrected for the pile-up of two or more photons. Under normal counting rates of 5 counts/sec, the pile-up correction was about 1.05. If the non-

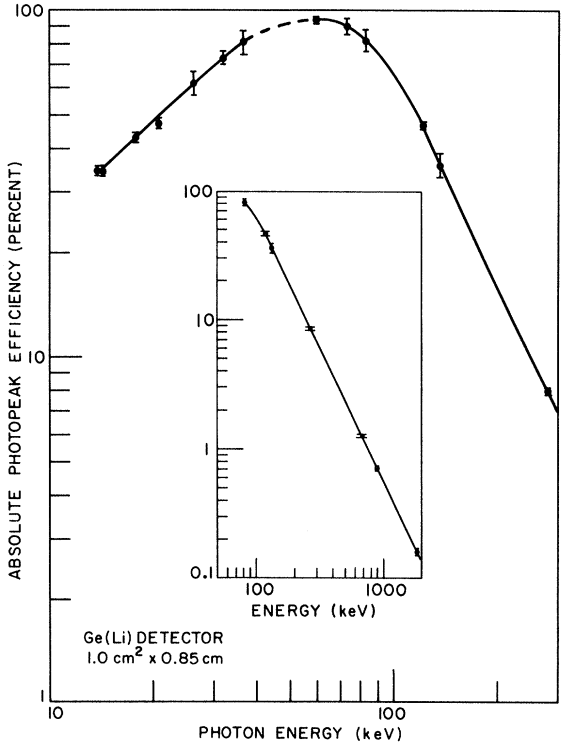

FIG. 7. Absolute photoelectric peak efficiency curve of the Ge(Li) detector. This curve has not been corrected for the escape of the Ge K x-rays.

uniformity in time of the beam were taken into account, this factor would be 0.25–0.8% larger.

B. Determination of Experimental Cross Sections

The differential cross section for a peak is given by

$$\left(\frac{d\sigma}{d\Omega}\right)_{\text{expt}} = \frac{N_\gamma}{N_e n_a \times \Delta\Omega \times C} \quad ,$$

where N_γ is the total number of photons emitted in the solid angle $\Delta\Omega$; n_a is the number of atoms per cm^2; N_e is the total number of incident electrons; $\Delta\Omega$ is the solid angle subtended by the detector; and C is the conversion factor, or the number of x rays or γ rays created per excitation event.

The number of photons N_γ is equal to the number of counts measured in the x- or γ-ray peak after background subtraction N_D, corrected for self-absorption, additional absorption prior to detection, detector efficiency, and counting-rate pile-up.

For the K-ionization experiment, the conversion factor C was the K-shell fluorescent yield f_y. In the γ-ray experiment, the conversion factor was

$$C = (1+\lambda_e/\lambda_\gamma)^{-1},$$

where λ_e is the probability per unit time that the nuclear multipole field will transfer its energy to an atomic electron, and λ_γ is the probability per unit time for photon emission by a radiative nuclear multipole transition.

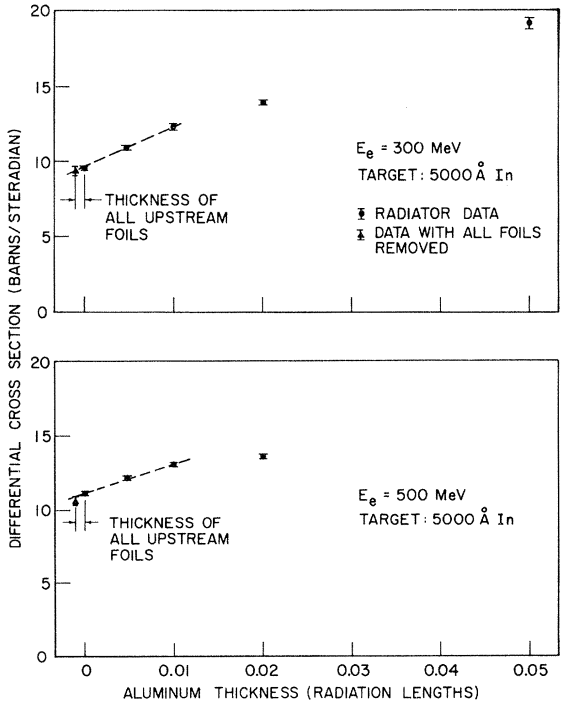

FIG. 8. Differential cross section of $_{49}$In for $\omega = 90°$ as a function of aluminum radiator thickness. (a) For incident electron energy of 300 MeV. (b) For incident electron energy of 500 MeV.

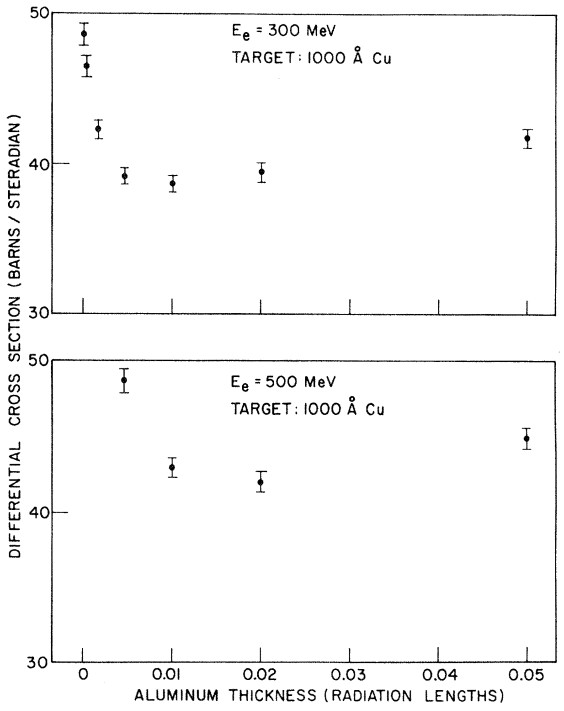

FIG. 9. Differential cross section of $_{29}$Cu for $\omega = 90°$ as a function of aluminum-radiator thickness. (a) For incident electron energy of 300 MeV. (b) For incident electron energy of 500 MeV.

C. Radiator Studies and Bremsstrahlung Corrections

By using aluminum radiators to create additional bremsstrahlung of known origin, a study was undertaken of the effect of the radiation accompanying the electron beam on the x-ray experiment. Radiators of varying thicknesses were placed upstream from the target, and the K-ionization cross section was measured as a function of radiator thickness. From the experimental curves, an estimate was obtained of the bremsstrahlung contributions of the upstream secondary emission monitor foils and the vacuum-protection foil totaling together 0.001 radiation length of aluminum.

Figures 8 and 9 show the K-ionization cross sections of $_{49}$In and $_{29}$Cu, measured at 90° from the direction of the incident electron beam, as a function of aluminum radiator thickness for electron energies of 300 and 500 MeV. Since the isotropy of cross section for x-ray production will be demonstrated later, it will suffice to review the results at 90°. The curves for $_{49}$In were not unexpected.

The aluminum radiators created bremsstrahlung in proportion to their thicknesses, and this radiation produced ionization within the targets. The curves appear to deviate from the expected linear relationship after the initial two hundredths of a radiation length. This was probably due to some absorption of low-energy bremsstrahlung within the thicker aluminum radiators.

The $_{29}$Cu cross-section curves in Figs. 9(a) and 9(b) generated considerable interest. They do not show the above-mentioned production, but instead demonstrate some apparent absorption. This indicated that the bremsstrahlung accompanying the beam was not entirely created by the aluminum in the upstream foils. Examination of these foils showed that they were not, in fact, made of pure aluminum but contained $_{29}$Cu, $_{30}$Zn, and perhaps $_{28}$Ni. The radiators used were made of 99.99% pure aluminum.

The pure-aluminum radiators were acting as absorbers of the bremsstrahlung just above the $_{29}$Cu K-ionization energy (8.98 keV) produced by these higher-Z elements, and the K x rays of the $_{30}$Zn impurity. The lower-intensity bremsstrahlung produced above the absorption edge of $_{49}$In (27.93 keV) by these impurities was not appreciably absorbed in the radiators. An experiment was performed at 300 MeV to test this hypothesis. The 72-in. spectrometer mount was rotated to 0° in order that the Si(Li) semiconductor detector looked directly along the beam pipe with the target removed. It was not possible to run the normal-intensity electron beam directly into the detector and cryostat because the electronic equipment would have been completely stalled by the enormous counting rate from incident electrons, photons, and scattered particles. In addition, serious damage and possible destruction of the detector would have resulted. Therefore, the experiment was performed with an rf electron beam generated by pulsing the accelerator without the electron gun grid or cathode voltage turned on. This provided the closest possible simulation that could be made to normal beam conditions.

The results of this experiment are shown in the series of Figs. 10(a)–10(f). These spectra have not been corrected for Mylar and air absorption. The experiment appears to confirm the hypothesis. The addition of radiators definitely decreased the intensity of the radiation above 8.98 keV and only slightly increased the intensity of the radiation above 27.93 keV [Figs. 10(a) and 10(b)]. Figures 10(b) and 10(c) show that as the radiators become thicker, the radiation above 8.98 keV, as well as that above 27.93 keV, began to rise again.

All spectra were collected for a fixed length of time and appear to be reproducible to within 5%.

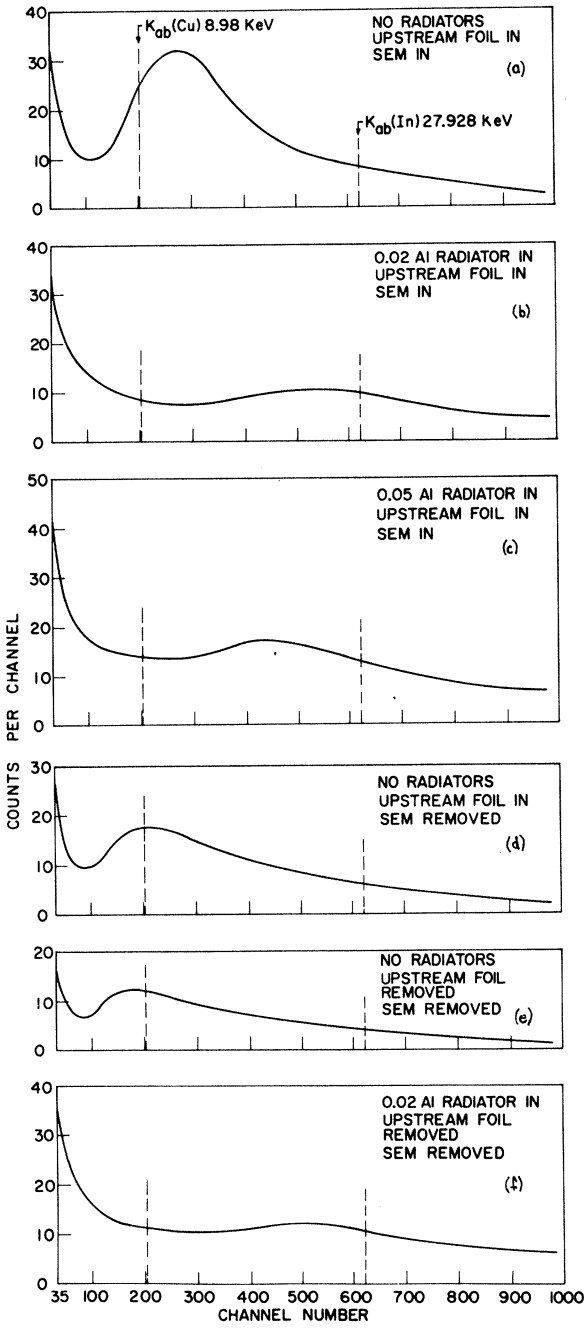

FIG. 10. Studies of photon spectra accompanying the 300-MeV electron rf-produced (electron gun off) beam were taken with various radiators and foils placed in the beam. The upstream foil was the vacuum protection foil.

The $_{29}$Cu K-ionization cross sections taken at 300 and 500 MeV after the removal of all foils and radiations were only 2% below the minima of Figs. 9(a) and 9(b), respectively. Similar $_{49}$In data resulted in cross sections which were within ± 3% of the extrapolated cross sections shown in Figs. 8(a)

TABLE I. K-ionization cross sections.

Target element	Detector	Thickness (mg/cm^2)	Differential cross sections (b/sr)[a] E_e = 150 MeV	300 MeV	500 MeV	700 MeV	900 MeV
$_{29}$Cu	Si(Li)	0.267	34.2 ±0.5	37.1 ±0.5	39.1 ±0.6	41.3 ±0.6	41.7 ±0.6
				36.9 ±0.45	38.5 ±0.6	40.8 ±0.5	40.7 ±0.6
		0.089		38.7 ±0.5	41.1 ±0.55		
					41.0 ±0.55		
		0.445		34.8 ±0.5			
				34.7 ±0.5			
				34.7 ±0.5			
$_{38}$Sr	Si(Li)	0.127	16.2 ±0.3	16.9 ±0.2	18.8 ±0.3	19.7 ±0.3	20.0 ±0.3
					18.1 ±0.3		
					18.3 ±0.3[b]		
$_{42}$Mo	Si(Li)	0.20	11.16 ±0.16	11.94 ±0.16	13.03 ±0.17	13.22 ±0.20	13.78 ±0.17
					12.67 ±0.17	13.07 ±0.17	

[a]Errors given are those due to counting statistics, charge collection, and pile-up correction.
[b]Ge(Li) detector used.

and 8(b). These studies led to the decision to run the cross-section experiments without any upstream protection foils.

An explicit determination of the contribution of the remaining beam bremsstrahlung to the K-ionization cross sections was made for $_{29}$Cu and $_{49}$In at 300 and 700 MeV. Holes 2 cm on a side were cut from the aluminum backing foil on both sides of the target-deposited area. The beam-steering coils deflected the electron beam through a hole and allowed only the uncharged particles to produce ionization. The cross sections from this experiment were less than 0.5% of the normal electron-beam-produced cross sections for $_{29}$Cu. No measurable $_{49}$In data above the background were present when the bremsstrahlung contribution to the $_{49}$In cross sections was studied. Therefore, the bremsstrahlung contribution appears to be less than 0.2% for $_{49}$In.

D. Error Analysis

A number of statistical and systematic errors contributed to the total or absolute uncertainty of any measurement made in these experiments. In the determination of photon cross sections, nine uncertainties were considered. The largest of these contributions were the uncertainties in the target thickness 5–10% and the detector full-energy peak efficiency 2.5–8%. The additional errors were due to uncertainties in the pile-up correction (0.8%), the transmission factor (1%, K x rays), the self-absorption (0.1%, K x rays), the solid angle (0.2%), the charge integration (1%), and the incident electron energy (0.5%). The peak area integration, which was used for detector-efficiency measurements as well as cross-section measurements, introduced an additional error. A thorough study of the uncertainties introduced by background subtraction, by choice of peak limits, by pile up, and by overlapping peaks has been made.[5]

The absolute uncertainty of the various x-ray intensity ratio measurements was independent of the target thickness, the current integration, the pile-up correction, and the solid-angle errors.

IV. K-IONIZATION EXPERIMENT

A. K-Ionization Cross Sections

The experimental differential K-ionization cross sections are presented in Tables I and II. Since all differential x-ray cross sections were found to be isotropic, the data were taken primarily at an angle of 90° measured from the beam direction. The error associated with each datum entry is due to counting statistics, pile-up correction, and charge integration only. This provides for a study of the reproducibility of the data and a comparison of the data as a function of energy for a given target. The absolute error, including the target-thickness error, of each element is approximately ±6%; for Ta and Mo the absolute error is about ±11%.

The data for 300 and 700 MeV are presented graphically as a function of atomic number for each incident electron energy in Figs. 11 and 12, respectively. The absolute errors are shown. Graphs for the data at 150, 500, and 900 MeV are similar. All of these log-log graphs show striking evidence for a power-law dependence of the differential cross section upon atomic number. For each electron energy, the slope, and thus the power of Z, is approximately −2.70. The power of Z is a constant as a function of incident electron energy over the range studied (150–900 MeV) to within ±0.02. Figures 13 and 14 display the energy dependence of the cross section for each element with the relative errors given in Tables I and II. A second-degree polynomial has been

TABLE II. K-ionization cross sections.

Target element	Detector	Thickness (mg/cm^2)	Differential cross sections (b/sr)[a] E_e = 150 MeV	300 MeV	500 MeV	700 MeV	900 MeV
$_{49}$In	Si(Li)	0.364	7.47 ± 0.10	8.53 ± 0.12	9.24 ± 0.12	9.41 ± 0.13	9.67 ± 0.12
					9.17 ± 0.14	9.36 ± 0.13	
		0.364		9.24 ± 0.13	10.09 ± 0.15		
				9.29 ± 0.12[b]	9.57 ± 0.13[b]	10.29 ± 0.14[b]	10.47 ± 0.14[b]
				9.30 ± 0.12[b]			
		0.053		9.14 ± 0.12			
$_{69}$Tm	Ge(Li)	2.18		3.57 ± 0.05	3.73 ± 0.05	3.83 ± 0.05	3.98 ± 0.05
				4.06 ± 0.07[c]		3.81 ± 0.05	
$_{73}$Ta	Ge(Li)	0.30		3.11 ± 0.04	3.30 ± 0.04		
					3.66 ± 0.13[c]		
$_{79}$Au	Ge(Li)	1.207		2.42 ± 0.03	2.52 ± 0.04	2.67 ± 0.04	2.74 ± 0.04
$_{83}$Bi	Ge(Li)	0.191		2.37 ± 0.04	2.56 ± 0.04		

[a]Errors given are those due to counting statistics, charge collection, and pile-up correction.

[b]Ge(Li) detector used.

[c]Si(Li) detector used.

fitted to the data for each element in Figs. 13 and 14. The energy range studied was 3×10^4–1×10^5 greater than the K-ionization energy for Cu, yet the cross section increased by only 11% within that range.

The differential K-ionization cross-section data have been compared to the theory of Kolbenstvedt.[2] This work is the most recent theoretical calculation performed and is in good agreement with a large number of earlier experimental data. For this theory, Kolbenstvedt calculated separately the contribution to the cross section from "near" collisions and from "distant" collisions. In his original work, he chose the impact parameter b to equal the K-shell atomic radius, as the point of transition between "near" and "distant" collisions with the atom. For distant collisions, Kolbenstvedt considered a spectrum of virtual photons having a field equivalent to the field of the impinging electron, as the electron passed the atomic nucleus. Kolbenstvedt employed the known scattering law between two free electrons as the in-

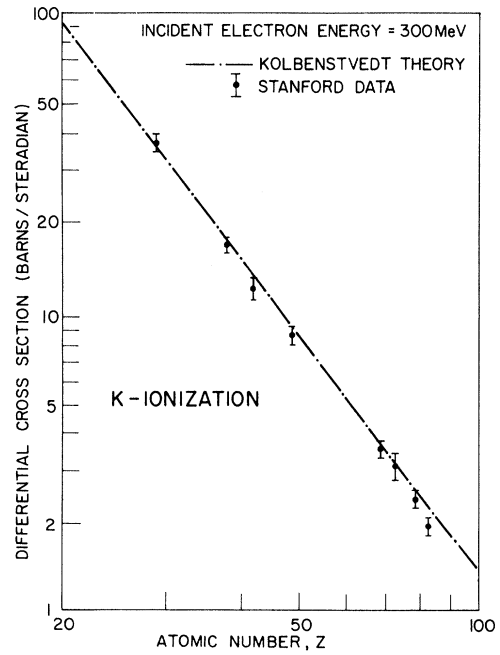

FIG. 11. Differential K-ionization cross section as a function of atomic number at $\omega = 90°$ and $E_e = 300$ MeV. The Kolbenstvedt theory is compared to the Stanford data points.

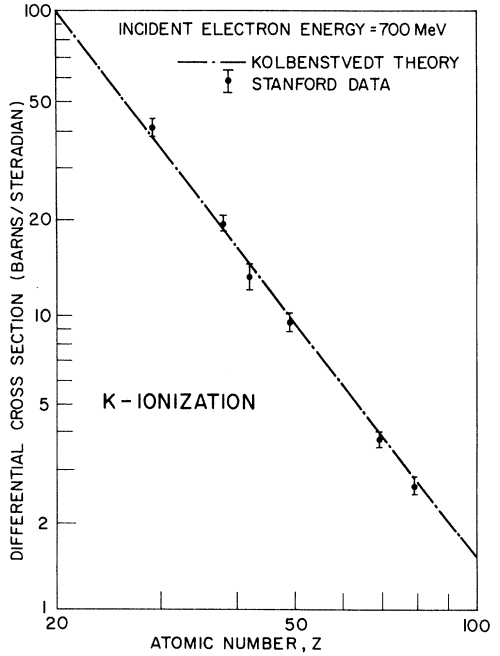

FIG. 12. Differential K-ionization cross section as a function of atomic number at $\omega = 90°$ and $E_e = 700$ MeV. The Kolbenstvedt theory is compared to the Stanford data points.

teraction for the close collisions. The total cross section is the sum of

$$\sigma_{\text{near}} = (0.275/I)[(E+1)^2/E(E+2)] \times \left[\ln\left(\frac{1.19E(E+2)}{I}\right) - \frac{E(E+2)}{(E+1)^2}\right] \quad (1)$$

and

$$\sigma_{\text{distant}} = (0.99/I)[(E+1)^2/E(E+2)] \times \left[1 - \frac{I}{E}\left(1 - \frac{E^2}{2(E+1)^2} + \frac{2E+1}{(E+1)^2}\ln\frac{E}{I}\right)\right],$$

where the cross sections are expressed in barns. The ionization energy I and the incident electron kinetic energy E are in electron rest-mass units. To compare this calculation with experiments, Kolbenstvedt has substituted the experimental ionization energies I_{expt} in place of $I = \frac{1}{2}(\alpha Z)^2$ in order to account for the effect of outer electron shells. Within the energy range of this experiment, this theoretical calculation provides a constant power-law dependence of the K-ionization cross section upon Z. The theoretical exponent is -2.31. This is compared to the experimentally determined power of -2.70 ± 0.02. The agreement is surprisingly good since extensive approximations were made in the theory for ease of computation. Recently, Kolbenstvedt[9] has reviewed his calculations in view of these results using ultrarelativistic electrons. He has noted that $q_0 = (2I_{\text{expt}})^{1/2}$ is the smallest possible momentum transfer in a free electron-electron collision (Møller collision) if the energy transfer is to exceed I_{expt}. Thus, he has chosen this value of q_0 as the cutoff and considered the two cases $q < q_0$ and $q > q_0$, separately.

For small momentum transfers, Kolbenstvedt has assumed that the incident and scattered electrons may be described by plane waves. This is valid for high incident energies and low-energy transfers which provide the largest contribution to the ionization process. The bound electron is described by a nonrelativistic Schrödinger wave function. With these assumptions and for $q \ll q_0$, the general matrix element reduces to the dipole approximation. The resulting contribution to the cross section from momentum transfers of $q < q_0$ is similar to the cross section calculated for "distant" collisions using the virtual photon approximation. In addition, the lower limit of integration is now I_{expt} rather than $I_0 = \frac{1}{2}(\alpha Z_{\text{eff}})^2$, where Z_{eff} is the effective charge. The result is

$$\sigma(q < q_0) = \frac{0.275}{I_{\text{expt}}}\left(\frac{I_0}{I_{\text{expt}}}\right)^3 \frac{(E+1)^2}{E(E+2)} \times \left\{\left[1 - \frac{16}{13}\left(1 - \frac{I_{\text{expt}}}{I_0}\right)\right]\right.$$

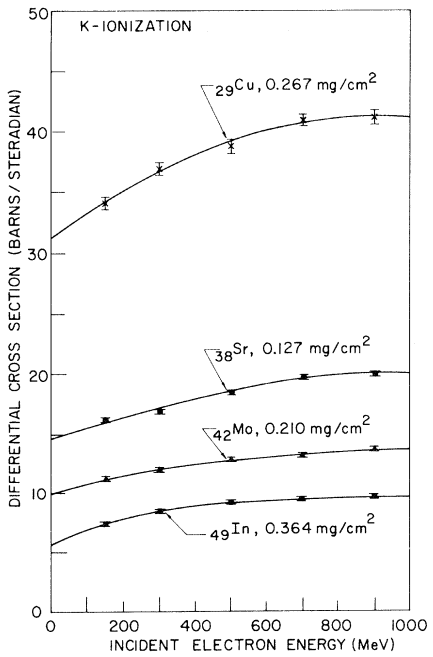

FIG. 13. Differential K-ionization cross section as a function of incident electron energy at $\omega = 90°$ for $_{29}$Cu, $_{38}$Sr, $_{42}$Mo, and $_{49}$In. A polynomial fit has been made to the data.

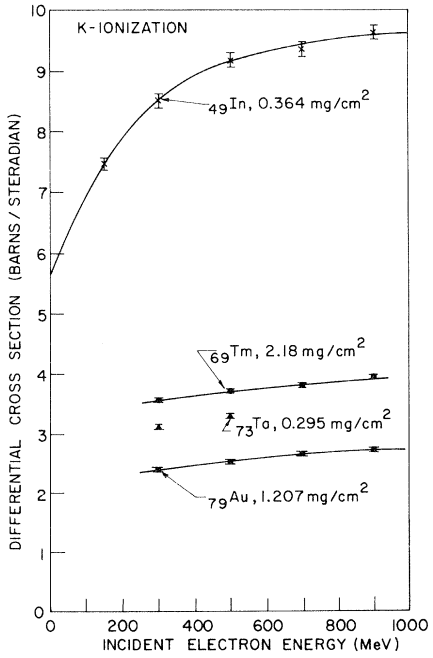

FIG. 14. Differential K-ionization cross section as a function of incident electron energy at $\omega = 90°$ for $_{49}$In, $_{69}$Tm, $_{73}$Ta, and $_{79}$Au. A polynomial fit has been made to the data.

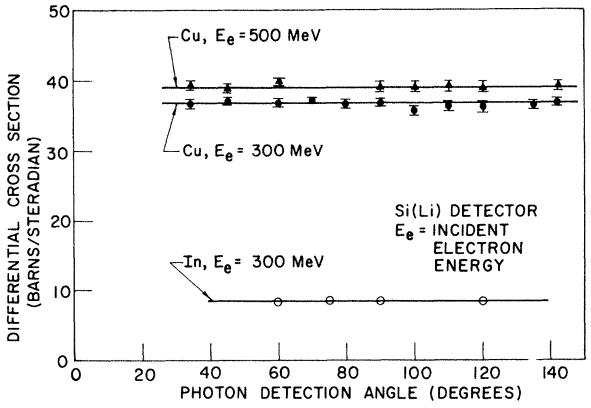

FIG. 15. Angular distribution of the differential K-ionization cross sections of $_{29}$Cu at 300 and 500 MeV and of $_{49}$In at 300 MeV.

$$\times\left(\ln\frac{2E(E+2)}{I_{\text{expt}}}-\frac{E(E+2)}{(E+1)^2}\right)-\frac{55}{78}$$

$$-\frac{32}{39}\left(1-\frac{I_{\text{expt}}}{I_0}\right)\Bigg\}\,.$$

For the $q \gg q_0$, the matrix element becomes approximately the same as in free electron-electron scattering. The result is given by Eq. (1). Kolbenstvedt has noted that in this calculation the dipole approximation ($q \ll q_0$) and the free electron-electron scattering approximation ($q \gg q_0$) have been extended into the region for $q \sim q_0$, where the approximations are poor. Thus, the region of momentum transfers of the order of q_0 should be investigated in future calculations.

A comparison of the experimental data with this recent calculation is provided in Figs. 11 and 12. The agreement is extremely good. The theoretical cross section now has a power-law dependence of $Z^{-2.60}$. The energy dependence of the experimental cross section of each element is also in excellent agreement with the Kolbenstvedt theory.

The contributions to the K x-ray and L x-ray yields produced by internal conversion are expected to be insignificant. This is substantiated by the theoretical estimates of nuclear excitation cross sections given below and the results of the γ-ray search. We did not differentiate between K ionization and K excitation to an outer shell.

B. Angular Distribution Studies of Cross Sections

Early in this experiment, a study was made of the angular distribution of the K-ionization cross sections of $_{29}$Cu and $_{49}$In. The results are shown in Fig. 15. The cross sections are isotropic to within the relative errors of ± 1.4%.

C. Intensity Ratios

The ratio of the $K\alpha$ intensity to the $K\beta$ intensity for each element was found to be independent of incident energy to within the statistical errors. A graph showing the results of the measurement of the $K\alpha/K\beta$ ratio as a function of atomic number is presented in Fig. 16 with the standard ratio curve of Wapstra *et al.*,[10] determined from the work of Williams[11] and Beckman.[12] Both Williams and Beckman observed the x rays produced by electron bombardment. Beckman estimated his errors to lie between ± 5 and ± 10%. The Stanford data, which have error estimates between ± 2.9 and 7.3%, appear to be consistently lower than the Wapstra curve for Z less than 72.

Recently, the $K\alpha/K\beta$ intensity ratios for Z = 29–92 have been measured by Slivinsky and Ebert.[13] They have used a high-resolution Ge(Li) detector to observe the x rays produced by exciting samples using the bremsstrahlung beam from a radiographic x-ray machine. Their data are plotted together with the Stanford data in Fig. 17. Better agreement exists between these data and the Stanford work than between either set and the Wapstra curve.

Also shown in Fig. 17 is the recent theoretical $K\alpha/K\beta$ intensity ratio curve determined from the relativistic Hartree-Slater calculations of radiative decay rates by Scofield.[14] Previous calculations include those by Massey and Burhop,[15] Ramberg and Richtmyer,[16] Asaad,[17] and Babushkin.[18] The theoretical curve of Scofield, which is in good agreement with Wapstra curves between Z = 30 and 68, is 5–10% higher than the Stanford-Slivinsky

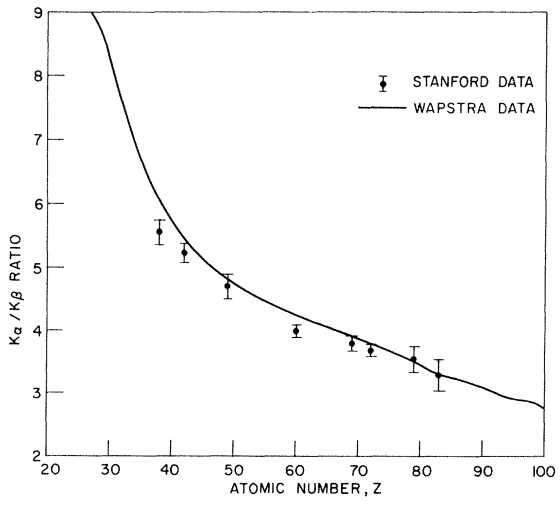

FIG. 16. Comparison of the $K\alpha/K\beta$ intensity ratios of the Stanford data with the Wapstra *et al.* data as a function of atomic number.

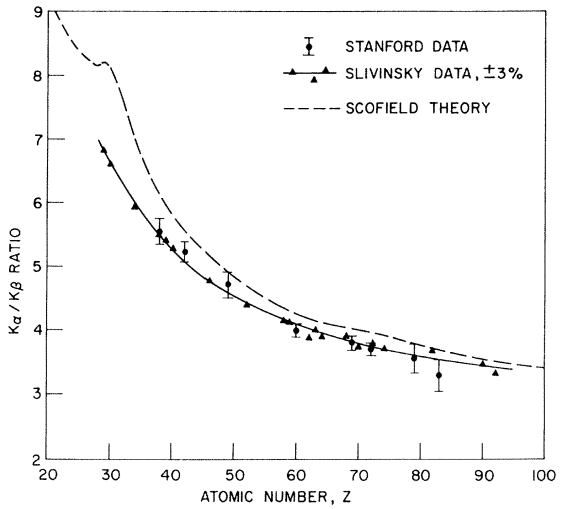

FIG. 17. Comparison of the $K\alpha/K\beta$ intensity ratios of the Stanford data with the Slivinsky-Ebert data and with the Scofield theory.

data. Recent calculations by Rosner and Bhalla[19] appear to agree with the Scofield values for low-Z elements.

For the highest-Z elements, the $K\alpha_1/K\alpha_2$ and $K\beta_1'/K\beta_2'$ intensity ratios were determined. Table III lists these ratios, with estimated errors of ± 5%, and those given by Wapstra *et al.*[10] and by Scofield.[14]

V. *L* X-RAY STUDIES

The L x-ray cross sections for four high-Z elements were determined using the Si(Li) detector. Since the $K\alpha$ and $K\beta$ x-ray lines were resolved in the data for the high-Z elements, it was possible to estimate the number of L-shell vacancies resulting from K ionizations. Even so, it was not possible to determine the L-ionization cross section because of the Coster-Kronig transitions $L_I \rightarrow L_{II}$, $L_{II} \rightarrow L_{III}$, and $L_I \rightarrow L_{III}$. These transitions result in rearrangements of the initial vacancy distribution of the three subshells. The L-fluorescent yields[20] are not accurately known and they are not the same for different subshells. Therefore, it is not simple to determine the relationship between the number of L x rays observed and the number of L ionizations produced.

TABLE III. K-shell intensity ratios.

Target element	Stanford	$K\alpha_1/K\alpha_2$ Wapstra	Scofield
$_{73}$Ta	1.6	1.85	1.74
$_{79}$Au	1.6	1.82	1.70
$_{83}$Bi	1.5	1.80	1.67
		$K\beta_1'/K\beta_2'$	
$_{73}$Ta	4.0	4.18	3.85
$_{79}$Au	3.6	3.73	3.59
$_{83}$Bi	3.4	3.37	3.39

TABLE IV. L x-ray cross sections.

Target element	Detector	Differential cross sections (b/sr)[a] E_e = 300 MeV	500 MeV	700 MeV	900 MeV
$_{69}$Tm	Si(Li)	20.7 ± 0.3	21.0 ± 0.3	21.3 ± 0.3	22.34 ± 0.3
$_{73}$Ta	Si(Li)	23.9 ± 0.3	24.9 ± 0.4	24.6 ± 0.4	25.1 ± 0.4
$_{79}$Au	Si(Li)	26.2 ± 0.4	27.4 ± 0.4	27.9 ± 0.4	29.0 ± 0.4
$_{83}$Bi	Si(Li)	29.2 ± 0.4	30.9 ± 0.4	31.0 ± 0.4	32.1 ± 0.5

[a]Errors given are those due to counting statistics, charge collection, and pile-up collection.

The average L x-ray cross sections for $_{69}$Tm, $_{73}$Ta, $_{79}$Au, and $_{83}$Bi are listed in Table IV for incident electron energies of 300, 500, 700, and 900 MeV. The relative errors shown provide a comparison of the results as a function of electron energy. Figure 18 is a graphic representation of this table. The x-ray cross section of each element increases slowly with energy; this energy dependence may be linear. It is interesting to note that

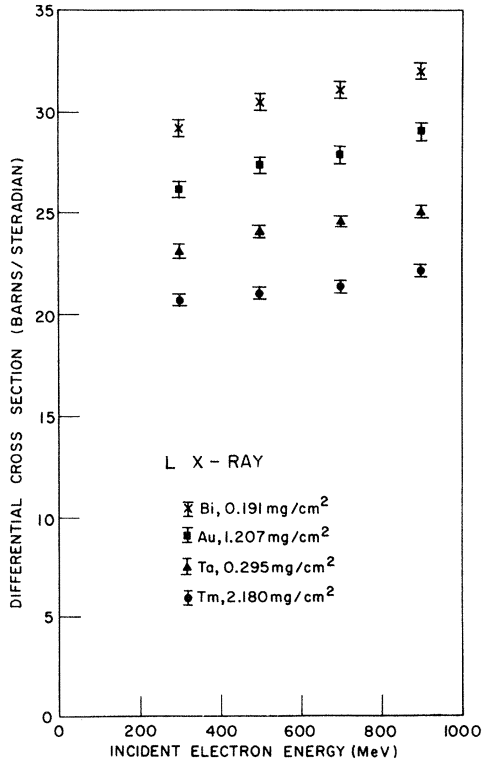

FIG. 18. Differential L x-ray cross section as a function of incident electron energy at $\omega = 90°$ for $_{83}$Bi, $_{79}$Au, $_{73}$Ta, and $_{69}$Tm.

TABLE V. Intensity ratios.

Target element	Electron energy (MeV)	K/L	$L\beta/L\alpha$	$L\gamma/L\alpha$
$_{69}$Tm	300	0.164	0.87	0.15
	500	0.166	0.84	0.15
	700	0.167	0.87	0.16
	900	0.167	0.86	0.15
$_{73}$Ta	300	0.126	0.87	0.17
	500	0.129	0.88	0.17
	700	···	0.88	0.17
	900	···	0.86	0.17
$_{79}$Au	300	0.088	0.80	0.15
	500	0.088	0.82	0.15
	700	0.091	0.80	0.14
	900	0.090	0.82	0.15
$_{83}$Bi	300	0.079	0.82	0.15
	500	0.079	0.84	0.15
	700	···	0.83	0.15
	900	···	0.84	0.15

the L x-ray cross section at any electron energy increases with Z while the K x-ray cross section decreases with Z.

The ratios of the K x-ray intensity to the L x-ray intensity for the four highest-Z targets used in these experiments are listed in Table V. It is interesting to note that the L x-ray cross sections are 6–13 times larger than the K x-ray cross sections for these high-Z materials. This ratio is a decreasing function of the atomic number, but for each element the ratio appears to be independent of incident electron energy. Thus, the K x-ray and L x-ray cross sections have a very similar dependence on the incident electron energy. The four peaks visible in the L spectra have been designated as the Ll, $L\alpha$, $L\beta$, and $L\gamma$ peaks in order of increasing energy. The ratios of the latter three peaks are presented in Table V. The most intense constituent lines of each peak are tabulated in Table VI, as identified by Storm and Israel[8] and by Scofield.[14] Here again, the ratios appear to be independent of incident electron energy. There seems to be some dependence on atomic number. However, the combined uncertainties of two L x-ray cross sections produce absolute errors in excess of 10%.

In high-energy particle studies, the equipment necessary to determine the ratio of the energy to the rest mass of a particle is usually expensive and cumbersome. One way to improve this situation might be to find a new means of studying the energy-loss process of a particle in matter. In the x-ray experiments performed at Stanford using electrons, we have noted that the K x-ray and L x-ray yields are energy dependent even at these high energies. The cross sections are also large; 20 b/sr is a representative value. Measurements of these cross sections may afford a rough way of determining the energy of other high-energy particles. Recently, Yuan *et al.*[21] made preliminary measurements of the transition radiation in the x-ray region. They have suggested this technique as a method for the determination of the relativistic factor γ.

TABLE VI. The intense lines contributing to the four observed L x-ray peaks.

Ll	l, t, s_1
$L\alpha$	α_1, α_2, η
$L\beta$	$\beta_1, \beta_2, \beta_3, \beta_4, \beta_{5/1}, \beta_6, \beta_7, \beta_{9/1}, \beta_{10}, \beta_{15}$
$L\gamma$	$\gamma_1, \gamma_2, \gamma_3, \gamma_{4/1}, \gamma_{4/2}, \gamma_5, \gamma_6, \gamma_8, \gamma_{9/2}, \gamma_{9/3}$

VI. γ-RAY STUDIES

Using semiconductor detectors, high-resolution studies of the γ-ray spectra produced by high-energy electron bombardment of nuclei might be performed. It was the purpose of this γ-ray experiment to determine the feasibility of such studies. The x-ray experiments showed that in the range of 5–100 keV, differential photon cross sections on the order of 10^{-24} cm^2/sr could be measured with a statistical error of ±1%. In this energy range, it was anticipated that differential cross sections on the order of 10^{-27} cm^2/sr could be observed using the present configuration.

Griffy and colleagues[3] estimated the total cross section for excitation of the $E2$ transition in $_{73}$Ta^{181} to be 7×10^{-28} cm^2 by using the plane-wave Born approximation. A search for nuclear γ lines was undertaken using $_{73}$Ta^{181} and $_{79}$Au^{197} as targets. Using 300- and 500-MeV incident electrons, spectra were taken at 45°, 90°, and 120°. The distinct photon energy ranges studied were 0–200 keV, 0–500 keV, and 50 keV to 2 MeV. No lines associated with the energy levels of $_{73}$Ta^{181} or $_{79}$Au^{197} were detected. However, a 511-keV γ line was observed. This line is associated with positron annihilation. At $\omega = 90°$, the differential cross section of this γ line for 300-MeV electrons incident upon a thick $_{79}$Au^{197} target was 1.1×10^{-26} cm^2/sr. This cross section appeared to be independent of the absorber thickness and thus confirmed the belief that the radiation was produced within the target itself. A study of the spectra confirmed that peaks having cross sections on the order of 10^{-27} cm^2/sr could be detected.

However, since the differential cross section of a nuclear line in $_{73}$Ta^{181} or $_{79}$Au^{197} was thought to be just below this level, the experiment was moved to the concrete vault opposite the 72-in. magnet. As a result of the larger background and the larger solid angle, the minimum differential cross

section measurable was 2×10^{-28} cm^2/sr. Again no nuclear photon lines of $_{73}Ta^{181}$ or $_{79}Au^{197}$ were present.

Since the conclusion of this search, Whitehill and Griffy[4] have calculated the differential cross sections for electron excitation of $_{73}Ta^{181}$ to the spin-$\frac{9}{2}^+$ state with excitation energy of 136 keV followed by γ decay to the ground state. These calculations estimate the differential cross sections at 120°, to be

$$\frac{d\sigma}{d\Omega}(E2) = 8.9\times10^{-29}\ \text{cm}^2/\text{sr}$$

and

$$\frac{d\sigma}{d\Omega}(M1) = 8.5\times10^{-29}\ \text{cm}^2/\text{sr}$$

for an incident electron energy of 200 MeV. Since their calculations assume that γ decay is the only deexcitation process, their results must be multiplied by the ratio

$$\Gamma_\gamma/(\Gamma_\gamma+\Gamma_e)\ ,$$

where Γ_γ is the partial width for γ decay and Γ_e is the partial width for internal conversion. This further reduces the estimated cross section by nearly $\frac{1}{3}$. It appears that these theoretical estimates are less than $\frac{1}{6}$ of the minimum measurable differential cross section. Our null result is thus not surprising.

In order to observe nuclear line spectra at the Mark-III accelerator, it will be necessary to use a larger detector. This detector should provide a greater solid angle and should have a larger relative efficiency at high energies.

VII. CONCLUSIONS

It has been demonstrated that semiconductor detectors are useful high-resolution detectors of photons produced by high-energy electron scattering. It was also suggested that with additional shielding and larger, more efficient Ge(Li) detectors, nuclear γ-ray spectra should also be observed. A data-analysis system employing the present on-line computer has been created. A method has been developed to correct the data for counting pile-up, and experimental studies of the effect of pile-up have been performed. A study of the low-energy bremsstrahlung spectra accompanying the electron beam has been made.

The new experimental data obtained include the measurement of the K-ionization cross section for a wide range of atomic numbers at high-incident electron energies. These energies were 1000–10 000 times the incident energies previously used. The cross section is an increasing function of incident electron energy, and has a dependence on Z proportional to $Z^{-2.70}$. The agreement between the theory of Kolbenstvedt and this experiment is very good. The L x-ray cross sections were determined for the target elements above $Z = 60$. Although the K x-ray and L x-ray cross sections have a similar energy dependence, the L x-ray cross sections, in contrast to the K x-ray cross sections, increase with atomic number. The intensity ratios $K\alpha_1/K\alpha_2$, $K\beta_1'/K\beta_2'$, $K\alpha/K\beta$, K/L, $L\beta/L\alpha$, and $L\gamma/L\alpha$ were found to be independent of incident electron energy, but were a function of the atomic number. These K-shell results were in agreement with recent low-energy data.

The measurement of the large x-ray cross sections or their ratios may afford a rough method for determining the ratio of the energy to the rest mass of other high-energy particles.

ACKNOWLEDGMENTS

We wish to express our appreciation to Dr. D. C. Sutton who gave assistance during the data runs and with the data analysis; to Dr. H. Kolbenstvedt, who provided additional theoretical calculations for the K-ionization experiment; and to Dr. T.A. Griffy and D. Whitehill, who sent us their unpublished theoretical calculations for the γ-ray experiment.

---

*Work supported in part by the U.S. Office of Naval Research Contract No. Nonr. 225(67), and by the National Science Foundation.

[1]J. W. Motz and R. C. Placious, Phys. Rev. 136, A662 (1964).

[2]H. Kolbenstvedt, J. Appl. Phys. 38, 4785 (1967).

[3]T.A. Griffy (private communications).

[4]D. Whitehill and T. A. Griffy (private communications).

[5]L. M. Middleman, Stanford University, Ph. D. thesis, 1969 (unpublished).

[6]H. R. Zulliger, L. M. Middleman, and D. W. Aitken, IEEE Trans. Nucl. Sci. NS-16, 47 (1969).

[7]See for example, E. Segrè, *Nuclei and Particles* (Benjamin, New York, 1964), p. 39.

[8]E. Storm and H. I. Israel, LASL Report No. LA-3753, 1967 (unpublished).

[9]H. Kolbenstvedt (private communications).

[10]A. H. Wapstra, G. J. Nijgh, and R. Van Lieshourt, *Nuclear Spectroscopy Tables* (North-Holland, Amsterdam, 1959), p. 81.

[11]J. H. Williams, Phys. Rev. 44, 146 (1933).

[12]O. Beckman, Arkiv Fysik 9, 495 (1955).

[13]V. W. Slivinski and P. J. Ebert, UCRL Report No. 71632, 1969 (unpublished).

[14]J. H. Scofield, UCRL Report No. 71424, 1968 (unpublished).

[15]H. S. W. Massey and E. H. S. Burhop, Proc. Cambridge Phil. Soc. 32, 461 (1936).
[16]E. G. Ramberg and F. K. Richtmyer, Phys. Rev. 51, 913 (1937).
[17]W. N. Asaad, Proc. Roy. Soc. (London) A249, 555 (1959).
[18]F. A. Babushkin, Opt. i Spektroskopiya 19, 3 (1965) [Opt. Spectry. (USSR) 19, 1 (1965)].
[19]H. R. Rosner and C. P. Bhalla, Bull. Am. Phys. Soc. 14, 183 (1969); and private communications.
[20]R. W. Fink, R. C. Jopson, H. Mark, and C. D. Swift, Rev. Mod. Phys. 38, 513 (1966).
[21]L. C. L. Yuan, C. L. Wang, and S. Prunster, Phys. Rev. Letters 23, 496 (1969).

PHYSICAL REVIEW A VOLUME 2, NUMBER 4 OCTOBER 1970

Molecular Coherence Effects in Radiation Processes: Bremsstrahlung

Edith Borie*
Institute of Physics, University of Trondheim, NLHT, Trondheim, Norway

and

National Bureau of Standards, Washington, D.C. 20234†

and

Leonard C. Maximon
National Bureau of Standards, Washington, D. C. 20234

and

Haakon Olsen
Institute of Physics, University of Trondheim, NLHT, Trondheim, Norway
(Received 17 February 1970; revised manuscript received 7 May 1970)

The influence of molecular structure on the bremsstrahlung process at low energies has been studied for diatomic molecules. Interference effects give rise to an increase in the total radiation cross section which is large for low electron energies. Although the various cross sections are calculated in Born approximation, the results are expected to be qualitatively correct.

I. INTRODUCTION

Molecular interference effects in low-energy electron scattering are well known and have been utilized extensively for molecular structure analysis.[1] It might be of interest to investigate whether the molecular structure may also have significant effects on radiation processes. In this paper we discuss the influence of the molecular structure of diatomic gases or liquids on the bremsstrahlung process at low electron energies. For simplicity, we consider diatomic molecules consisting of identical atoms. In addition, we treat the process in first Born approximation and account for the effects of the atomic electrons by assuming independent atoms with simple exponential screening, thus neglecting molecular binding. Although the cross sections calculated in this manner are only approximately correct, it is expected that, except for extremely small momentum transfers, the interference effects in the exact cross sections are closely similar.[2]

The importance of molecular interference effects in a scattering or radiation process is determined by the magnitude of the momentum $\vec{q}$ transferred to the molecule. In order that interference effects be large, the wavelength corresponding to q, viz., $\lambda_q = \hbar/q$, should be of the order of or larger than the interatomic spacing R. The momentum transfer is given by

$$\vec{q} = \vec{p}_1 - \vec{p}_2 - \vec{k} \tag{1}$$

and thus varies in magnitude between the values $q_{\min}$ and $q_{\max}$, where

$$q_{\max} = p_1 + p_2 + E_1 - E_2\,, \quad q_{\min} = p_1 - p_2 - (E_1 - E_2) \tag{2}$$

and $\vec{p}_1, \vec{p}_2, \vec{k}$, E_1, and E_2 are defined below in (8). For high energies, $q_{\min} = k/(2E_1E_2)$, and the smallness of this quantity gives rise to the coherence effect in high-energy bremsstrahlung.[3] For low energies we have $p_1 \ll mc$, and (2) simplifies to